AFRL-RV-PS-
TR-2008-1030

AFRL-RV-PS-
TR-2008-1030

Effects of Electronic Quantum Interference, Photonic-Crystal Cavity, Longitudinal Field and Surface-Plasmon-Polariton for Optical Amplification

D.A. Cardimona, Paul M. Alsing, and Danhong Huang

9 April 2008

Interim Report

AIR FORCE RESEARCH LABORATORY
Space Vehicles Directorate
3550 Aberdeen Ave SE
AIR FORCE MATERIEL COMMAND
KIRTLAND AIR FORCE BASE, NM 87117-5776

DTIC COPY

NOTICE AND SIGNATURE PAGE

AFRL-RV-PS-TR-2008-1030 HAS BEEN REVIEWED AND IS APPROVED FOR PUBLICATION IN ACCORDANCE WITH ASSIGNED DISTRIBUTION STATEMENT.

//signed//

DAVID CARDIMONA
Program Manager

//signed//

JOHN P. BEAUCHEMIN, Lt Col, USAF
Deputy Chief, Spacecraft Technology Division
Space Vehicles Directorate

REPORT DOCUMENTATION PAGE

Form Approved
OMB No. 0704-0188

1. REPORT DATE *(DD-MM-YYYY)*	**2. REPORT TYPE**	**3. DATES COVERED** *(From - To)*
09/04/2008	Interim Report	09/01/2006 to 09/04/2008

4. TITLE AND SUBTITLE
Effects of Electronic Quantum Interference, Photonic-Crystal Cavity, Longitudinal Field and Surface-Plasmon- Polariton for Optical Amplification

5a. CONTRACT NUMBER

5b. GRANT NUMBER

5c. PROGRAM ELEMENT NUMBER

6. AUTHOR(S)
D.A. Cardimona, Paul M. Alsing, and Danhong Huang

5d. PROJECT NUMBER

5e. TASK NUMBER

5f. WORK UNIT NUMBER

7. PERFORMING ORGANIZATION NAME(S) AND ADDRESS(ES)

Air Force Research Laboratory
Space Vehicles Directorate
3550 Aberdeen Ave., SE
Kirtland AFB, NM 87117-5776

8. PERFORMING ORGANIZATION REPORT NUMBER
AFRL-RV-PS-TR-2008-1030

9. SPONSORING / MONITORING AGENCY NAME(S) AND ADDRESS(ES)

10. SPONSOR/MONITOR'S ACRONYM(S)

11. SPONSOR/MONITOR'S REPORT NUMBER(S)

12. DISTRIBUTION / AVAILABILITY STATEMENT
Approved for public release; distribution is unlimited. (Clearance #VS06-0701).

13. SUPPLEMENTARY NOTES

14. ABSTRACT

Some possibilities for coherent optical amplification of a normally-incident and weak radiation field are reviewed based on various physical mechanisms, such as electronic quantum interference induced by a coupling laser field in a three-level system, field enhancement through the cavity confinement of a radiation field in a photonic crystal and field concentration seen in a transmitted near field through a metallic surface grating due to excitation of surface-plasmon-polariton modes. Numerical results are presented and discussed to demonstrate these inter-esting effects. The important role played by a longitudinal field resulting from the absorption by an induced three-dimensional plasma wave inside a doped semiconductor is analyzed using a nonlocal and non-adiabatic model.

15. SUBJECT TERMS
amplification, quantum interference, surface-plasmon-polariton, photonic crystal, longitudinal field

16. SECURITY CLASSIFICATION OF:			**17. LIMITATION OF ABSTRACT**	**18. NUMBER OF PAGES**	**19a. NAME OF RESPONSIBLE PERSON**
a. REPORT	**b. ABSTRACT**	**c. THIS PAGE**			D.A. Cardimona
Unclassified	Unclassified	Unclassified	Unlimited	15	**19b. TELEPHONE NUMBER** *(include area code)*

Standard Form 298 (Rev. 8-98)
Prescribed by ANSI Std. 239.18

Effects of Electronic Quantum Interference, Photonic-Crystal Cavity, Longitudinal Field and Surface-Plasmon-Polariton for Optical Amplification

Danhong Huang, D. A. Cardimona and Paul M. Alsing

(Invited paper)

***Abstract*— Some possibilities for coherent optical amplification of a normally-incident and weak radiation field are reviewed based on various physical mechanisms, such as electronic quantum interference induced by a coupling laser field in a three-level system, field enhancement through the cavity confinement of a radiation field in a photonic crystal and field concentration seen in a transmitted near field through a metallic surface grating due to excitation of surface-plasmon-polariton modes. Numerical results are presented and discussed to demonstrate these interesting effects. The important role played by a longitudinal field resulting from the absorption by an induced three-dimensional plasma wave inside a doped semiconductor is analyzed using a nonlocal and non-adiabatic model.**

***Index Terms*— amplification, quantum interference, surface-plasmon-polariton, photonic crystal, longitudinal field.**

I. Introduction

ELECTRONIC quantum interference in a multi-level atomic system can originate from the superposition of a direct transition of electrons and an indirect transition of electrons mediated by a self-absorption of spontaneous photons after a probe field is applied resonantly. A complete theory [1] for the radiative decay of excited electrons in an atomic system requires a full quantum electrodynamic treatment of both the electromagnetic (EM) field and the electrons. Using this approach one finds that in addition to the usual diagonal radiative-decay process, there exists an off-diagonal radiative-decay coupling (ODRDC) effect that becomes very important when two or more electron transition energies are very close [2]. The ODRDC effect describes a nearly-resonant absorption of a spontaneously emitted photon from the downward transition of one electron by another electron that subsequently transits upward to a close-by different level. By properly tuning the frequency of a laser field that couples the ground state to two excited states, the phase-sensitive coherence between the two upper levels, which is provided by the ODRDC process, adds an equivalent "*population*" to one of the two excited states. When this coherence is strong enough, an incoming probe field resonant with the transition between a meta-stable level and one of the two upper levels can be amplified via a stimulated emission process. A similar quantum interference effect provides the framework for electromagnetically induced transparency (EIT) [3], which has attracted a lot of attention and has been confirmed experimentally [4]. The scheme proposed to observe EIT uses a Fano-type interference [5], [6] between a pair of coherently prepared dressed states. In this paper, we will restrict our comparison to Harris's EIT scheme [3] unless otherwise indicated. Since the early proposal for studying effects of electronic quantum interference in semiconductor quantum wells [7], there have been a lot of researches on EIT and lasing without inversion in semiconductor systems.

Recently, there has been growing interest in studies of the propagation of EM waves in disordered and/or periodic dielectric structures [8]. This interest is partly due to the possibility of observing the localization of EM waves in disordered dielectric structures [9]−[13] and also to the possible existence of photonic band gaps in three-dimensional (3D) periodic dielectric structures [14]−[20]. In analogy to the case of an electron wave propagating in a crystal, light waves traveling in periodic structures will be described in terms of photonic bands with the possibility of the existence of frequency gaps where the propagation of EM waves is forbidden. In the original proposal for photonic band structures [16], it was suggested that the inhibition of spontaneous emission in such gaps can be utilized to substantially enhance the performance of semiconductor lasers and detectors. Surprisingly, the very recently observed black-body-type emission from 3D metallic photonic crystals displayed unique spectrum [21].

Ebbesen *et al.* [22] reported a relatively enhanced optical transmission seen in arrays of subwavelength cylindrical holes in metallic films. Similar phenomena have been observed in subwavelength metallic gratings [23] and even in simple planar metallic films [24]. These enhanced optical transmissions are believed to be related to light coupling to surface-plasmon-polariton (SPP) modes in non-structured [24] or structured [25] metallic films. The observation of tunable localized surface plasmons was also reported in a nanodot-liquid crystal matrix [26]. In order to understand the physics involved in the enhanced optical transmission, near-field calculations are required. The previously-proposed calculational methods include a modal expansion [25], the Chandezon method [27], a simplified analytical method [28], and a finite-difference time-domain method [29]. All these methods are spatially local and adiabatic in time, thereby neglecting the nonlocal dynamic relationship [30], [31] between the induced material polarization and the total EM field in the Maxwell equations, but can be applied to dielectric host materials in which there are no free charged carriers. In addition, the absorption from the longitudinal field due to the induced plasma wave in

metals [32] has been neglected, which tends to underestimate the loss of SPP waves propagating along the interface between air and metals.

In its simplest form an SPP is an EM excitation that propagates in a wave-like fashion along the planar interface between a metal and a dielectric medium and whose amplitude decays exponentially with increasing distance into each medium from the interface [33]−[35]. Thus, an SPP is a surface EM wave, whose field is confined to the near vicinity of the dielectric-metal interface. This confinement leads to an enhancement of the field at the interface [36], resulting in an extraordinary sensitivity of the SPP to surface conditions. Surface plasmon polariton-based devices exploiting this sensitivity are widely used in chemo- and bio-sensors [37]. The enhancement of the EM field at the interface is responsible for surface-enhanced optical phenomena such as Raman scattering, second harmonic generation, fluorescence, *etc* [33], [38]. The relative ease of manipulating SPPs on a surface opens an opportunity for their applications to photonics and optoelectronics for scaling down optical and electronic devices to nanometric dimensions [39]. The intrinsically two-dimensional nature of SPPs prohibits them from directly coupling to light. Usually, a surface metal grating is required for the excitation of SPPs by normally-incident light through an interaction between SPPs and the grating. Moreover, since the EM field of an SPP decays exponentially with distance from the surface, it cannot be observed in conventional (far-field) experiments unless the SPP is transformed into light by its interaction with a surface grating.

In this paper, we will review coherent optical amplification of a normally-incident and weak radiation field based on various physical mechanisms, including electronic quantum interference in a three-level system, field enhancement in a photonic-crystal cavity and field concentration of a transmitted near field through a metallic surface grating. The important role played by a longitudinal field resulting from an induced three-dimensional plasma wave will also be analyzed.

The rest of the paper is as follows. In Sec. II, we discuss the effects of electronic quantum interference on optical absorption through either off-diagonal radiative-decay coupling or electromagnetically-induced transparency. In Sec. III, we discuss the photonic band gaps in periodic dielectric structures and the cavity enhancement of an incident radiation field used as a coupling field for electromagnetically-induced transparency in a quantum dot. In Sec. IV, we discuss the important optical absorption by a longitudinal field inside conducting materials and its effect on the transmitted near field. In Sec. V, we discuss the field concentration through a metallic surface grating and the excitation of surface plasmon polaritons through the interaction with either a prism or a grating. The paper is briefly concluded in Sec. VI.

II. Electronic Quantum Interference

In Fig. 1(a), we consider a three-level system with two nearly degenerate upper levels. In this case, the equations for the density matrix $[\rho_{ij}]$ of the system in Fig. 1(a) are [40]

$$-2\beta_{21,\ 12}\ \rho_{22}-\Omega_{12}^{\rm R}\ Im\left(\rho_{12}\right)-2\beta_{21,\ 13}\ Re\left(\rho_{23}\right)=0\ , \quad (1)$$

$$-2\beta_{31,\ 13}\ \rho_{33}-\Omega_{13}^{\rm R}\ Im\left(\rho_{13}\right)-2\beta_{31,\ 12}\ Re\left(\rho_{23}\right)=0\ , \quad (2)$$

$$i\left(\omega_{21}-\omega_{\rm p}\right)\rho_{12}-\beta_{21,\ 12}\ \rho_{12}+\frac{i\Omega_{12}^{\rm R}}{2}\left(\rho_{22}-\rho_{11}\right) +\frac{i\Omega_{13}^{\rm R}}{2}\ \rho_{23}^{*}-\beta_{21,\ 13}\ \rho_{13}=0\ , \quad (3)$$

$$i\left(\omega_{31}-\omega_{\rm p}\right)\ \rho_{13}-\beta_{31,\ 13}\rho_{13}+\frac{i\Omega_{13}^{\rm R}}{2}\left(\rho_{33}-\rho_{11}\right) +\frac{i\Omega_{12}^{\rm R}}{2}\ \rho_{23}-\beta_{31,\ 12}\ \rho_{12}=0\ , \quad (4)$$

$$i\omega_{32}\ \rho_{23}-\left(\beta_{21,\ 12}+\beta_{31,\ 13}\right)\rho_{23}+\frac{i\Omega_{12}^{\rm R}}{2}\ \rho_{13} -\frac{i\Omega_{13}^{\rm R}}{2}\ \rho_{12}^{*}-\left(\beta_{31,\ 12}\ \rho_{22}+\beta_{21,\ 13}\ \rho_{33}\right)=0\ , \quad (5)$$

where $\Omega_{ij}^{\rm R}=2e\mathcal{E}_{\rm p}r_{ij}/\hbar$ is the resonant Rabi frequency, $\mathcal{E}_{\rm p}$ and $\omega_{\rm p}$ are the amplitude and tfrequency of the probe field, $\hbar\omega_{ij}$ is the energy separation between levels i and j, and $\beta_{ij,mn}$ stands for the diagonal and off-diagonal radiative-decay rates between levels i and j coupled by a dipole moment er_{ij}.

In Fig. 1(b), we consider another three-level system with the upper two levels resonantly coupled by a pump laser with a frequency $\omega_{\rm L}$ and an amplitude $\mathcal{E}_{\rm L}$. In this case, however, the density-matrix equations for the dressed system in Fig. 1(b) are [40]

$$-\Gamma_2\ \rho_{22}-\Omega_{12}^{\rm R}\ Im\left(\rho_{12}\right)-\sqrt{\Gamma_2\Gamma_3}\ Re\left(\rho_{23}\right)=0\ , \quad (6)$$

$$-\Gamma_3\ \rho_{33}-\Omega_{13}^{\rm R}\ Im\left(\rho_{13}\right)-\sqrt{\Gamma_2\Gamma_3}\ Re\left(\rho_{23}\right)=0\ , \quad (7)$$

$$i\left(\omega_{21}-\omega_{\rm p}\right)\rho_{12}-\frac{1}{2}\ \Gamma_2\ \rho_{12} +\frac{i\Omega_{12}^{\rm R}}{2}\left(\rho_{22}-\rho_{11}\right)+\frac{i\Omega_{13}^{\rm R}}{2}\ \rho_{23}^{*}-\frac{1}{2}\ \sqrt{\Gamma_2\Gamma_3}\ \rho_{13}=0\ , \quad (8)$$

$$i\left(\omega_{31}-\omega_{\rm p}\right)\rho_{13}-\frac{1}{2}\ \Gamma_3\ \rho_{13}+\frac{i\Omega_{13}^{\rm R}}{2}\left(\rho_{33}-\rho_{11}\right) +\frac{i\Omega_{12}^{\rm R}}{2}\ \rho_{23}-\frac{1}{2}\ \sqrt{\Gamma_2\Gamma_3}\ \rho_{12}=0\ , \quad (9)$$

$$i\omega_{32}\ \rho_{23}-\frac{1}{2}\left(\Gamma_2+\Gamma_3\right)\rho_{23} +\frac{i\Omega_{12}^{\rm R}}{2}\ \rho_{13}-\frac{i\Omega_{13}^{\rm R}}{2}\ \rho_{12}^{*}-\frac{1}{2}\ \sqrt{\Gamma_2\Gamma_3}\left(\rho_{22}+\rho_{33}\right)=0\ , \quad (10)$$

where $\Gamma_2=\Gamma_3^{(0)}\sin^2\theta$ and $\Gamma_3=\Gamma_3^{(0)}\cos^2\theta$ are the decay rates from dressed levels 2 and 3 to the lower continuum

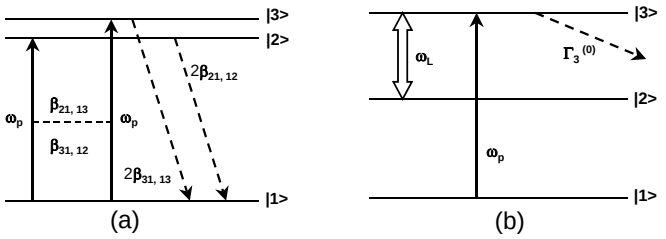

Fig. 1. Schematic illustrations for the effects of (a) off-diagonal radiative-decay coupling (ODRDC) and (b) electromagnetically-induced transparency (EIT) in the bare-atom picture. Here, $\omega_{\rm L}$ stands for the frequency of a strong coupling laser field, $\omega_{\rm p}$ stands for the frequency of probe field. The notations $|1>$, $|2>$ and $|3>$ represent different energy states in the bare-atom picture. The dashed arrows denote the decay processes, while the solid arrows represent the excitations induced by the probe fields. The double hollow arrow represents the level coupling established by an external laser field. The symbols $\beta_{ij,mn}$ are defined in the text. $\Gamma_3^{(0)}$ is the decay rate to a continuum state outside of the system. The ODRDC in (a) is denoted by the horizontal dashed line.

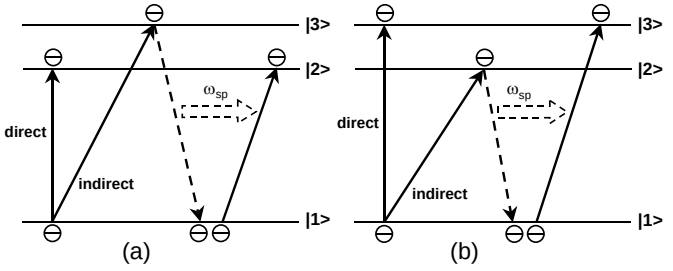

Fig. 2. Schematic illustrations for the quantum interference between the direct absorption path and indirect absorption path involving a $\beta_{21,\ 13}$-ODRDC process in (a) and a $\beta_{31,\ 12}$-ODRDC process in (b), where $\omega_{\rm sp}$ and the horizontal hollow arrows stand for the spontaneous photon emitted by radiative decay of one electron and then absorbed by the other electron. The symbol ◯ with "−" at its center stands for an electron. This type of quantum interference is responsible for the zero absorption from the ground level to two nearly-resonant upper levels at a certain frequency.

state, $\omega_{21} = [\omega_{21}^{(0)} + \omega_{31}^{(0)} + \omega_{\rm L} - \Omega_{\rm R}]/2$, $\omega_{31} = [\omega_{21}^{(0)} + \omega_{31}^{(0)} + \omega_{\rm L} + \Omega_{\rm R}]/2$, $r_{12} = -r_{13}^{(0)}\sin\theta$, $r_{13} = r_{13}^{(0)}\cos\theta$, $\Omega_{\rm R} = \sqrt{(\omega_{32}^{(0)} - \omega_{\rm L})^2 + (\Omega_{23}^{\rm c})^2}$, $\Omega_{ij}^{\rm R} = 2e\mathcal{E}_{\rm p} r_{ij}/\hbar$, $\Omega_{23}^{\rm c} = 2e\mathcal{E}_{\rm L} r_{23}^{(0)}/\hbar$ and $\tan 2\theta = \Omega_{23}^{\rm c}/(\omega_{\rm L} - \omega_{32}^{(0)})$. The superscript (0) refers to the corresponding quantities in the bare-atom picture.

As shown in Fig. 2 for the system in Fig. 1(a) we understand that the electronic quantum interference comes from the superposition of a direct absorption path to one upper level and an indirect absorption path through another upper level followed by an off-diagonal radiative decay and ending in the same final state as the direct path [41]. This electronic quantum interference is formally described by $|A + B\exp(i\phi)|^2$ with transition amplitudes A and B and phase difference ϕ for the two different paths. When $\omega_{21} < \omega_{\rm p} < \omega_{31}$, $\phi = \pi$ can be reached and $A = B$ can be satisfied at the same time. This leads to a complete destructive interference which gives rise to a zero absorption.

As shown in Fig. 3 for the system in Fig. 1(b), we see that the existence of the electronic quantum interference is also due

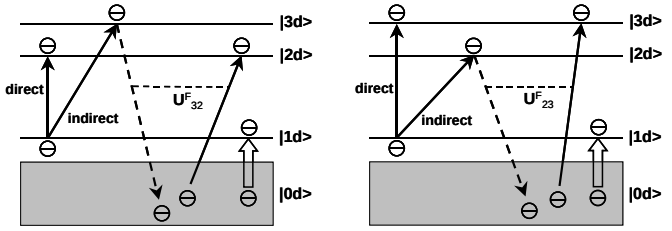

Fig. 3. Schematic illustrations for the quantum interference in the dressed-atom picture between the direct absorption path and indirect absorption path involving two different Fano-type couplings in (a) and (b), where the vertical hollow arrows stand for the electrons pumped from the continuum state $|0d>$ (reservoir shown by the shaded region) to the ground state $|1d>$. The Fano-type interaction $U_{32}^{\rm F} = U_{23}^{\rm F}$ couples two discrete states through a decay to the continuum state, which transfers energy from a decayed electron to the excitation of an electron from the continuum state to one of the two upper dressed states $|2d>$ and $|3d>$. This type of quantum interference is responsible for the EIT from the ground level to one of the two laser-coupled upper levels in the bare-atom picture, as shown in Fig. 1(b).

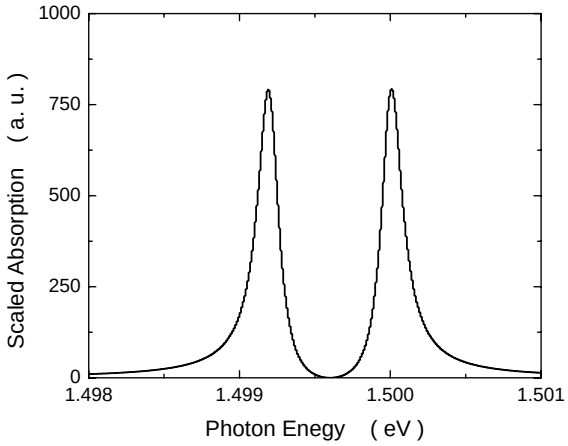

Fig. 4. Calculated scaled absorption coefficient in arbitrary unit (a.u.) as a function of the probe photon energy $\hbar\omega_{\rm p}$ for the ODRDC effect without electron scattering.

to a superposition of a direct absorption path and an indirect absorption path mediated by an energy transfer which takes energy from a decayed electron to the continuum and gives it back to another electron excited out of the continuum via a so-called Fano coupling [5], [40]. To maintain the $|1d>$-level population, a pumping laser is needed for moving electrons to $|1d>$ from the continuum state $|0d>$.

For the numerical results, shown in Fig. 4 [41], we choose $\hbar\omega_{31} = 1.5\ eV$, $\hbar\omega_{32} = 8\times10^{-4}\ eV$, $r_{12} = r_{13} = 6\ \mathring{A}$, and $\mathcal{E}_{\rm p} = 1\ kV/cm$ for the system in Fig. 1(a). In the absence of electron scattering, we find a zero absorption of the probe field at $\omega_{\rm p} = (\omega_{21} + \omega_{31})/2$ as a result of the equal dipole moments $r_{12} = r_{13}$. This directly comes from the superposition of the direct absorption path and indirect absorption path, as shown in Fig. 2. The peak width is determined by the power broadening proportional to $\Omega_{12}^{\rm R} = \Omega_{13}^{\rm R}$.

Electron scattering is found to create a dephasing to the induced optical coherence ρ_{ij} with $i \neq j$. When the dephasing rate becomes comparable to the Rabi fre-

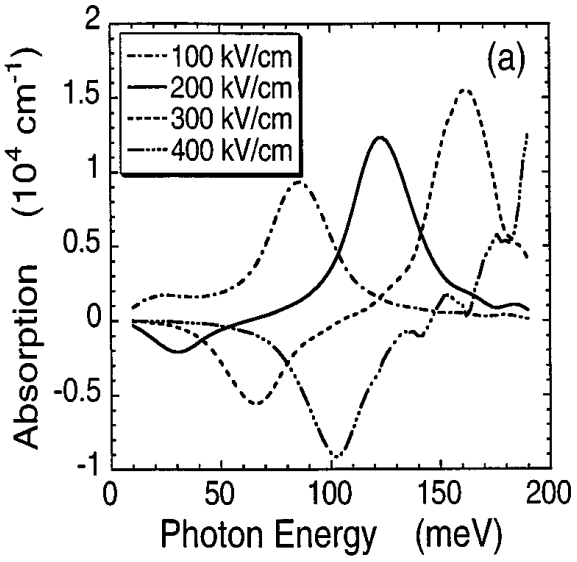

Fig. 5. Plot of the time-averaged optical spectrum with different coupling laser strengths $\mathcal{E}_{\rm L} = 100,\ 200,\ 300\ 400\ kV/cm$. Here, we have taken $T = 4\ K$, $L_{\rm W} = 150\ \mathring{A}$, $n_{\rm 2D} = 1.5 \times 10^{12}\ cm^{-2}$ (doping in the well), $\hbar\omega_{\rm L} = E_3(0) - E_2(0)$, $\tau_{23}(k;\ t) = 28\ fs$, $\tau_j^{\rm rel}(k;\ t) = 45\ fs$ for $j = 1,\ 2,\ 3$, $\tau_{12}(k;\ t) = 132\ fs$, $\tau_{13}(k;\ t) = 36\ fs$, $T_{\rm pulse} = 200\ fs$ and $t_{\rm D} = 0$.

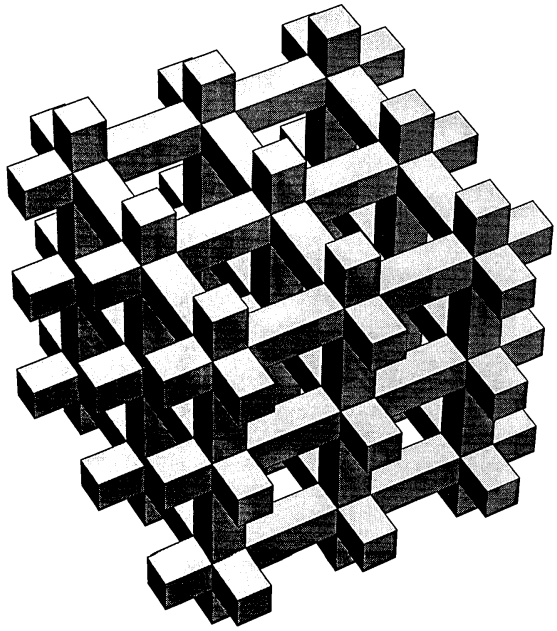

Fig. 6. Square-rod structure. A $3 \times 3 \times 3$ section is shown. Image used with permission of authors of [43].

quency $\Omega_{23}^{\mathcal{E}}$ of the coupling laser, the electronic quantum interference in the system in Fig. 1(b) will be destroyed [42]. However, the suppressed electronic quantum interference will be recovered when the intensity of the coupling laser is increased, as shown in Fig. 5, where a three-level $Al_{0.25}Ga_{0.75}As/GaAs/Al_{0.4}Ga_{0.6}As$ asymmetric quantum well is considered [42].

III. Photonic-Crystal Cavity

For a three-dimensional dielectric photonic crystal, the band structure of photons is determined by the Maxwell equations

$$\vec{\nabla} \times \left[\frac{1}{\epsilon_{\rm r}(\vec{r})} \vec{\nabla} \times \vec{H}(\vec{r}) \right] = \frac{\omega^2}{c^2} \vec{H}(\vec{r}) \ , \qquad (11)$$

where the dielectric function $\epsilon_{\rm r}(\vec{r})$ takes values of either 1 for air or $\epsilon_{\rm b}$ for the dielectric medium, and is a periodic function in the three-dimensional space. Since $\epsilon_{\rm r}(\vec{r})$ is periodic, we can use Bloch's theorem to expand the transverse $\vec{H}$ field in plane waves [20],

$$\vec{H}(\vec{r}) = \sum_{\vec{G}} \sum_{\lambda=1}^{2} h_{\vec{G},\lambda} \vec{e}_\lambda \exp[i(\vec{k} + \vec{G}) \cdot \vec{r}] \ , \qquad (12)$$

where $\vec{k}$ is a wave vector in the Brillouin zone of the lattice, $\vec{G}$ is a reciprocal-lattice vector, and $\vec{e}_1,\ \vec{e}_2$ are unit vectors perpendicular to $\vec{k}+\vec{G}$. Substituting Eq. (12) into Eq. (11) leads to the following equation for an eigen-vector $h_{\vec{G},\lambda}$

$$\sum_{\vec{G}',\lambda'} M_{\vec{G},\vec{G}'}^{\lambda,\lambda'} h_{\vec{G}',\lambda'} = \frac{\omega^2}{c^2} h_{\vec{G},\lambda} \ , \qquad (13)$$

where

$$M_{\vec{G},\vec{G}'}^{\lambda,\lambda'} = |\vec{k}+\vec{G}||\vec{k}+\vec{G}'| \epsilon_{\vec{G},\vec{G}'}^{-1} \begin{bmatrix} \vec{e}_2 \cdot \vec{e}_{2'} & -\vec{e}_2 \cdot \vec{e}_{1'} \\ -\vec{e}_1 \cdot \vec{e}_{2'} & \vec{e}_1 \cdot \vec{e}_{1'} \end{bmatrix} \qquad (14)$$

and $\epsilon_{\vec{G},\vec{G}'} = \epsilon_{\rm r}(\vec{G} - \vec{G}')$ is the Fourier transform of $\epsilon_{\rm r}(\vec{r})$.

For a simple-cubic lattice of square-rods, as shown in Fig. 6, the photon dispersion relation [43]) is displayed in Fig. 7, where an absolute band gap is denoted by the shaded bar in the figure.

When a single defect is intentionally introduced in the photonic crystal, a photonic-crystal cavity is formed. Within the cavity, photon modes are localized with energy inside the band gap. As a generalization of Eq. (11), the Maxwell equations become [44]

$$\vec{\nabla} \times \left\{ \left[\frac{1}{\epsilon_{\rm r}(\vec{r})} + U(\vec{r}) \right] \vec{\nabla} \times \vec{H}(\vec{r}) \right\} = \frac{\omega^2}{c^2} \vec{H}(\vec{r}) \ , \qquad (15)$$

where $U(\vec{r}) = -\epsilon_{\rm d}(\vec{r}) / \{\epsilon_{\rm r}(\vec{r})[\epsilon_{\rm r}(\vec{r}) + \epsilon_{\rm d}(\vec{r})]\}$ and $\epsilon_{\rm d}(\vec{r})$ is the dielectric function of the cylindrical defect. In Fig. 8, we show a top view for the calculated cavity-field distribution in a two-dimensional photonic crystal with punched holes in a dielectric film, from which we can clearly see the localization of the cavity radiation field inside the defect region. This spatial localization of the field greatly enhances the amplitude of the field inside the cavity.

The great enhancement of the cavity radiation field inside the cavity can be used as a strong coupling field to produce an electronic quantum interference in quantum dots placed in the cavity, as shown in Fig. 9, where an incident light field is expected to be amplified as much as a million times by a high-Q cavity and then used as the coupling field resonant with two upper levels in a quantum dot.

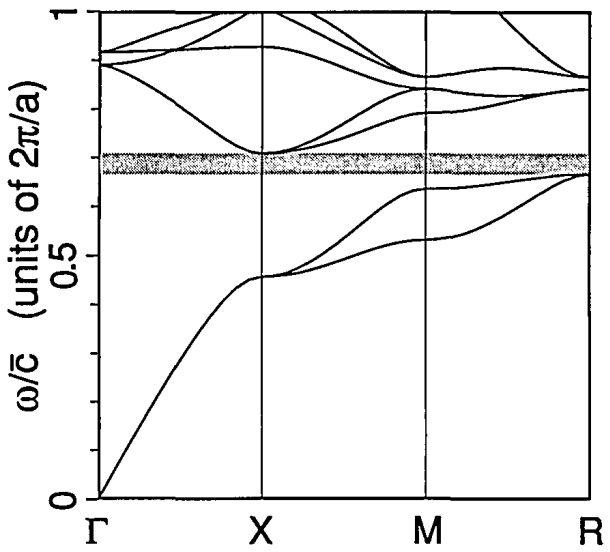

Fig. 7. Photonic bands for the square-rod structure in the simple-cubic lattice with $\epsilon_2 = 13$ for dielectric, $\epsilon_1 = 1$ for air and $\beta = 0.82$. Image used with permission of authors of [43].

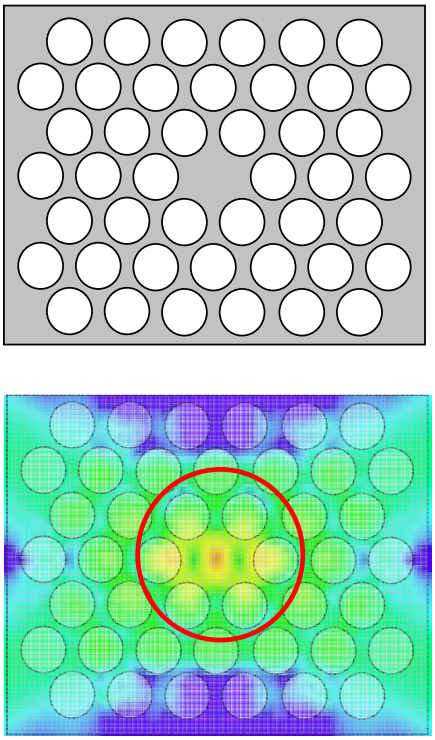

Fig. 8. Top views of a two-dimensional photonic-crystal cavity (upper panel) formed by removing a hole from a dielectric film, and the spatial distribution of the electric field (lower panel) in the photonic crystal formed by using the dielectric film ($\epsilon_r = 12$) punched with an array of holes ($\epsilon_r = 1$), where $\epsilon_d = 12$ and the spread of the cavity radiation field inside the photonic crystal is denoted by a circle.

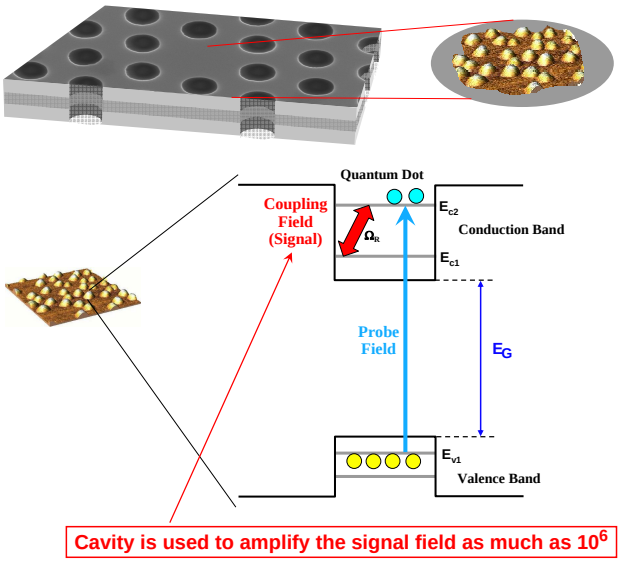

Fig. 9. The upper panel illustrates self-assembled InAs/GaAs quantum dots buried inside a two-dimensional photonic-crystal cavity. The lower panel shows the band structure for one of buried quantum dots, where two upper conduction sublevels are resonantly coupled by a strong cavity radiation field and a probe field is coupled to the second conduction sublevel and the top valence sublevel, similar to the system in Fig. 1(b).

IV. Longitudinal-Field Effect

For a system with a half space of air ($z < 0$) and a half space of a doped semiconductor ($z > 0$) toped with a conducting sheet at $z = 0$, the formal solution to the Maxwell wave equations can be formally written as

$$\begin{bmatrix} \vec{E}(\vec{q}_\parallel, \omega,\ z) \\ \vec{H}(\vec{q}_\parallel, \omega,\ z) \end{bmatrix} = \exp(i\beta_1^{\rm T} z) \begin{bmatrix} \vec{A}^{\rm T}_{(+)}(\vec{q}_\parallel, \omega) \\ \vec{B}^{\rm T}_{(+)}(\vec{q}_\parallel, \omega) \end{bmatrix} + \exp(-i\beta_1^{\rm T} z) \begin{bmatrix} \vec{A}^{\rm T}_{(-)}(\vec{q}_\parallel, \omega) \\ \vec{B}^{\rm T}_{(-)}(\vec{q}_\parallel, \omega) \end{bmatrix} \quad \text{for } z < 0\ , \tag{16}$$

and

$$\begin{bmatrix} \vec{E}(\vec{q}_\parallel, \omega,\ z) \\ \vec{H}(\vec{q}_\parallel, \omega,\ z) \end{bmatrix} = \exp(i\beta_2^{\rm T} z) \begin{bmatrix} \vec{C}^{\rm T}_{(+)}(\vec{q}_\parallel, \omega) \\ \vec{D}^{\rm T}_{(+)}(\vec{q}_\parallel, \omega) \end{bmatrix} + \exp(i\beta_2^{\rm L} z) \begin{bmatrix} \vec{C}^{\rm L}_{(+)}(\vec{q}_\parallel, \omega) \\ 0 \end{bmatrix} \quad \text{for } z > 0\ , \tag{17}$$

where the complex transverse wave numbers $\beta^{\rm T}_{1,2}$ are given by the transverse dielectric function $\epsilon^{\rm T}_{1,2}(\vec{q}_\parallel, \beta^{\rm T}_{1,2},\ \omega)$ through

$$\begin{bmatrix} \{\beta_1^{\rm T}(\vec{q}_\parallel,\ \omega)\}^2 \\ \{\beta_2^{\rm T}(\vec{q}_\parallel,\ \omega)\}^2 \end{bmatrix} = \frac{\omega^2}{c^2} \begin{bmatrix} 1 \\ \epsilon_2^{\rm T}(\vec{q}_\parallel, \beta_2^{\rm T},\ \omega) \end{bmatrix} - q_\parallel^2\ . \tag{18}$$

Here $\epsilon_1^{\rm T}(\vec{q}_\parallel, \beta_1^{\rm T},\ \omega) = 1$ is taken for the air side. On the other hand, the complex longitudinal wave number $\beta_2^{\rm L}$ inside the doped semiconductor is determined by the zero of the longitudinal dielectric function, *i.e.* $\epsilon_2^{\rm L}(\vec{q}_\parallel, \beta_2^{\rm L},\ \omega) = 0$. The transverse (T) field is perpendicular to $\vec{q} = (\vec{q}_\parallel,\ \beta)$, while the longitudinal (L) field is parallel to $\vec{q}$.

In the presence of a conducting sheet at the interface $z = 0$, the boundary conditions of the fields $\{\vec{E},\ \vec{H}\} = \{\vec{E}^{\rm T} + \vec{E}^{\rm L},\ \vec{H}^{\rm T}\}$are [45]

$$\vec{E}^{\rm T}_{x,y}(\vec{q}_\parallel,\omega,\ 0^+)+\vec{E}^{\rm L}_{x,y}(\vec{q}_\parallel,\omega,\ 0^+) = \vec{E}^{\rm T}_{x,y}(\vec{q}_\parallel,\omega,\ 0^-)\ , \quad (19)$$

$$\begin{aligned}&\epsilon^{\rm T}_2(\vec{q}_\parallel,\beta^{\rm T}_2,\ \omega)]E^{\rm T}_z(\vec{q}_\parallel,\omega,\ 0^+) - E^{\rm T}_z(\vec{q}_\parallel,\omega,\ 0^-)\\ &= \frac{1}{\epsilon_0}\left[\rho_{\rm s}(\vec{q}_\parallel,\ \omega) - iq_xP^x_{\rm s}(\vec{q}_\parallel,\ \omega) - iq_yP^y_{\rm s}(\vec{q}_\parallel,\ \omega)\right]\ , \quad (20)\end{aligned}$$

$$\begin{aligned}&H^{\rm T}_x(\vec{q}_\parallel,\omega,\ 0^+) - H^{\rm T}_x(\vec{q}_\parallel,\omega,\ 0^-)\\ &= -i\omega P^y_{\rm s}(\vec{q}_\parallel,\ \omega) + \alpha^y_{\rm s}(\vec{q}_\parallel,\ \omega)\ , \quad (21)\end{aligned}$$

$$\begin{aligned}&H^{\rm T}_y(\vec{q}_\parallel,\omega,\ 0^+) - H^{\rm T}_y(\vec{q}_\parallel,\omega,\ 0^-)\\ &= i\omega P^x_{\rm s}(\vec{q}_\parallel,\ \omega) - \alpha^x_{\rm s}(\vec{q}_\parallel,\ \omega)\ , \quad (22)\end{aligned}$$

$$H^{\rm T}_z(\vec{q}_\parallel,\omega,\ 0^+) = H^{\rm T}_z(\vec{q}_\parallel,\omega,\ 0^-)\ , \quad (23)$$

where $\vec{P}_{\rm s}$, $\rho_{\rm s}$ and $\vec{\alpha}_{\rm s}$ are the sheet polarization, sheet charge density and sheet current density, respectively. The existence of the longitudinal field inside the doped semiconductor bulk requires a supplementary boundary condition [45], given by

$$\begin{aligned}&-i\omega\epsilon_0\left[\epsilon^{\rm T}_2(\vec{q}_\parallel,\beta^{\rm T}_2,\ \omega) - \epsilon_{\rm b}\right]E^{\rm T}_z(\vec{q}_\parallel,\omega,\ 0^+)\\ &+i\omega\epsilon_0\epsilon_{\rm b}E^{\rm L}_z(\vec{q}_\parallel,\omega,\ 0^+)\\ &= i\vec{q}_\parallel\cdot\left[\vec{\alpha}_{\rm s}(\vec{q}_\parallel,\ \omega) + \frac{\partial\vec{P}_{\rm s}(\vec{q}_\parallel,\ \omega)}{\partial t}\right]\ . \quad (24)\end{aligned}$$

Considering the rotational symmetry of the system, we can take $q_y = 0$ for our calculation. Therefore, the transfer matrix becomes [32] (see top of the next page)

where $q_x = (\omega/c)\sin\theta_{\rm i}$, $\theta_{\rm i}$ is the incident angle, $\bar{\chi}_{\rm s} = \bar{\chi}^*_{\rm s} + (\epsilon_{\rm s}-1)\Delta L$, $\epsilon_{\rm s}$ and ΔL are the sheet dielectric constant and thickness, and $\bar{\chi}^*_{\rm s}(q_x,\ \omega)$ will be defined below. By using the matrix in Eq. (24), the solution for the s-polarization fields can be expressed as

$$\begin{bmatrix} B^{\rm T}_x\\ B^{\rm T}_y\\ C^{\rm T}_x\\ C^{\rm T}_y\\ C^{\rm L}_x\end{bmatrix}_{\rm s} = \underline{\mathcal{M}}^{-1}_{\rm t}\otimes\begin{bmatrix}0\\ -A_y\\ (\bar{\chi}_{\rm s} - i\beta^{\rm T}_1c^2/\omega^2)A_y\\ 0\\ 0\end{bmatrix}\ , \quad (26)$$

and the solution for the p-polarization fields is expressed as

$$\begin{bmatrix} B^{\rm T}_x\\ B^{\rm T}_y\\ C^{\rm T}_x\\ C^{\rm T}_y\\ C^{\rm L}_x\end{bmatrix}_{\rm p} = \left(\frac{1}{\omega\epsilon_0}\right)\ \underline{\mathcal{M}}^{-1}_{\rm t}\otimes\begin{bmatrix}-\beta^{\rm T}_1A_y\\ 0\\ 0\\ (\beta^{\rm T}_1\bar{\chi}_{\rm s} - i)A_y\\ 0\end{bmatrix}\ . \quad (27)$$

Based on these solutions, the square ratios of the reflected field (r) and the transmitted field (t) to the incident field for both s- and p-polarization are

$$\begin{aligned}&\begin{bmatrix} F_{\rm rs}(q_x,\ \omega)\\ F_{\rm ts}(q_x,\ \omega)\end{bmatrix}\\ &= \begin{bmatrix}\frac{(1+|q_x/\beta^{\rm T}_1|^2)|B^{\rm T}_x|^2+|B^{\rm T}_y|^2}{A^2_y}\\ \frac{|C^{\rm L}_x+C^{\rm T}_x|^2+|C^{\rm T}_y|^2+|(\beta^{\rm L}_2/q_x)C^{\rm L}_x-(q_x/\beta^{\rm T}_2)C^{\rm T}_x|^2}{A^2_y}\end{bmatrix}_{\rm s}\ , \quad (28)\\ &\begin{bmatrix} F_{\rm rp}(q_x,\ \omega)\\ F_{\rm tp}(q_x,\ \omega)\end{bmatrix}\\ &= \left(\frac{\epsilon_0}{\mu_0}\right)\begin{bmatrix}\frac{1+|q_x/\beta^{\rm T}_1|^2)|B^{\rm T}_x|^2+|B^{\rm T}_y|^2}{A^2_y}\\ \frac{|C^{\rm L}_x+C^{\rm T}_x|^2+|C^{\rm T}_y|^2+|(\beta^{\rm L}_2/q_x)C^{\rm L}_x-(q_x/\beta^{\rm T}_2)C^{\rm T}_x|^2}{A^2_y}\end{bmatrix}_{\rm p}\ . \quad (29)\end{aligned}$$

For the doped semiconductor, its optical properties are described by the longitudinal and transverse dielectric functions [45]

$$\frac{\epsilon^{\rm L}_2(q_x,q_z,\omega)}{\epsilon_{\rm b}} = 1 - \frac{n_{3{\rm D}}e^2}{\epsilon_0\epsilon_{\rm b}m^*[\omega(\omega+i\gamma_0) - \xi(q^2_x+q^2_z)]}\ , \quad (30)$$

$$\frac{\epsilon^{\rm T}_2(q_x,\ \omega)}{\epsilon_{\rm b}} = 1 - \frac{n_{3{\rm D}}e^2}{\epsilon_0\epsilon_{\rm b}m^*\omega(\omega+i\gamma_0)}\ , \quad (31)$$

where $\xi = 3v^2_{\rm F}/5$ and $v_{\rm F} = \hbar(3\pi^2n_{3{\rm D}})^{1/3}/m^*$. On the other hand, the sheet optical properties are described by the sheet polarizability [46]

$$\bar{\chi}_{\rm s}(q_x,\ \omega) = -\frac{n_{2{\rm D}}e^2}{\omega(\omega+i\gamma'_0)\epsilon_0m^*_{\rm s}} + (\epsilon_{\rm s}-1)\Delta L\ . \quad (32)$$

In Fig. 10, we choose $n_{3{\rm D}} = 10^{17}\ cm^{-3}$, $m^*/m_0 = 0.067\ m_0$, $\epsilon_{\rm b} = \epsilon_{\rm s} = 12$, $\Delta L = 30\ \mathring{A}$, $n_{2{\rm D}} = 1.326\times 10^{13}\ cm^{-2}$ and $m^*_{\rm s} = 0.024\ m_0$. Other parameters are indicated in the figure captions. Figure 10 displays $F_{\rm tp}$ for the p polarization as a function of $\hbar\omega$. Results for p polarization are compared for three different cases: (1) including both a longitudinal field (LF) and a conducting sheet (solid curve); (2) including only a conducting sheet but not a longitudinal field (dash-dot-dotted curve); (3) including only a longitudinal field but not a conducting sheet, (dashed curve). We expect to see only one resonance around $\hbar\Omega^{\rm pl}_{3{\rm D}} = 13.1\ meV$ in $F_{\rm tp}$. In the absence a longitudinal field, the resonant frequency of $F_{\rm tp}$ is obtained by minimizing $|\Re e\left\{\beta^{\rm T}_2 + \beta^{\rm T}_1\epsilon^{\rm T}_2 + i\beta^{\rm T}_1\beta^{\rm T}_2\bar{\chi}_{\rm s}(q_x,\ \omega)\right\}|$ at $\omega = \omega_{\rm r}$. In Fig. 10, the peak of the dash-dot-dotted curve reflects the resonance determined by $\omega = \omega_{\rm r}$. After the longitudinal field is included, the peak strength (solid curve) is reduced due to the strong absorption by the longitudinal 3D plasma wave, and its peak position is slightly shifted down. On the other hand, the peak strength of the dashed curve is significantly increased when the conducting sheet is excluded due to absence of the strong

$$\underline{\mathcal{M}}_{\rm t}=\left[\begin{array}{ccccc} 1 & 0 & -1 & 0 & -1 \\ 0 & 1 & 0 & -1 & 0 \\ 0 & -\bar{\chi}_{\rm s}-i\beta_1^{\rm T}c^2/\omega^2 & 0 & -i\beta_2^{\rm T}c^2/\omega^2 & 0 \\ -\bar{\chi}_{\rm s}-i/\beta_1^{\rm T} & 0 & -i\epsilon_2^{\rm T}/\beta_2^{\rm T} & 0 & 0 \\ 0 & 0 & (q_x/\beta_2^{\rm T})(\epsilon_2^{\rm T}-\epsilon_{\rm b})+iq_x\bar{\chi}_{\rm s}^* & 0 & (\beta_2^{\rm L}/q_x)\epsilon_{\rm b}+iq_x\bar{\chi}_{\rm s}^* \end{array}\right], \quad (25)$$

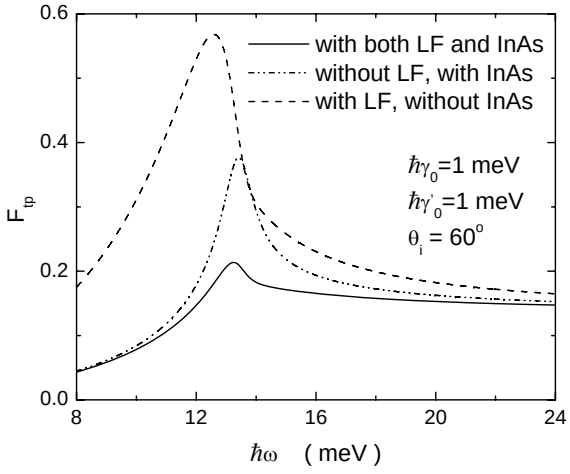

Fig. 10. Calculated $F_{\rm tp}$ for the p polarization as a function of the incident photon energy $\hbar\omega$ with $\theta_{\rm i}=60^{\rm o}$, $\hbar\gamma_0=1\ meV$, and $\hbar\gamma_0'=1\ meV$. The results of $F_{\rm tp}$ are compared for three different cases: (1) including both a longitudinal field (LF) and an InAs conducting sheet (solid curve); (2) without a longitudinal field but with an InAs conducting sheet (dash-dot-dotted curve); (3) without an InAs conducting sheet ($n_{\rm 2D}=0$) but with a longitudinal field (dashed curve).

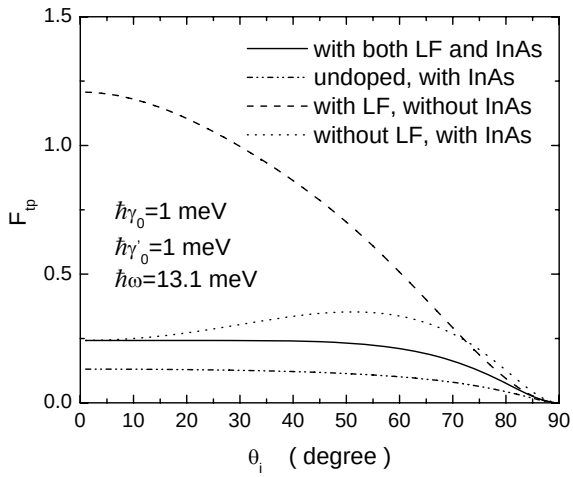

Fig. 11. Calculated $F_{\rm tp}$ for the p polarization as a function of $\theta_{\rm i}$ with $\hbar\omega=\hbar\Omega_{\rm 3D}^{\rm pl}=13.1\ meV$, $\hbar\gamma_0=1\ meV$, and $\hbar\gamma_0'=1\ meV$. The results of $F_{\rm tp}$ are compared for four different cases: (1) including both a longitudinal field and an InAs conducting sheet (solid curve); (2) with an undoped GaAs bulk ($n_{\rm 3D}=0$) and with an InAs conducting sheet (dash-dot-dotted curve); (3) without an InAs conducting sheet but with a longitudinal field (dashed curve); (4) without a longitudinal field but with an InAs conducting sheet (dotted curve).

reflection by the sheet current. In addition, the peak position of the dashed curve is shifted down due to the excitation of the longitudinal 3D plasma wave with an energy slightly lower than $\hbar\Omega_{\rm 3D}^{\rm pl}$.

We choose the same parameters for the calculation in Fig. 11. From it we see the effects of a conducting sheet and a doped bulk on the angular distribution as a function of $\theta_{\rm i}$. Results for p polarization are compared for four different cases: (1) with a longitudinal field, a conducting sheet and a doped bulk (solid curve); (2) with a conducting sheet and an undoped bulk (dash-dot-dotted curve); (3) with a longitudinal field and a doped bulk but without a conducting sheet (dashed curve); (4) with a conducting sheet and a doped bulk but without a longitudinal field (dotted curve). From Fig. 11 we see that free electrons in the doped bulk increase $F_{\rm tp}$ over that of the undoped bulk at $\theta_{\rm i}=0^{\rm o}$. When $\theta_{\rm i}=90^{\rm o}$, $F_{\rm tp}=0$. The difference in values of $F_{\rm tp}$ at $\theta_{\rm i}=0^{\rm o}$ for doped and undoped bulk is caused by free electrons, which leads to $|\epsilon_2^{\rm T}|\ll\epsilon_{\rm b}$ for the doped bulk compared with $\epsilon_{\rm b}$ of the undoped bulk. The inclusion of the conducting sheet greatly reduces $F_{\rm tp}$ due to strong reflection. The longitudinal field only slightly reduces $F_{\rm tp}$ when $\theta_{\rm i}>20^{\rm o}$. $F_{\rm tp}>1$ (dashed curves) is seen when conducting sheet is absent, as well as $\theta_{\rm i}<30^{\rm o}$.

V. Surface-Plasmon-Polariton

Considering a smooth air-metal interface, if the longitudinal field is neglected inside the metal with conductivity $\sigma_{\rm c}\to\infty$, we can solve the Maxwell wave equations along with proper boundary conditions. In the absence of a longitudinal field and a conducting sheet at the interface, Eqs. (26) and (27) lead us to the following analytical solutions for the transmitted and reflected fields with p- and s-polarization

$$\left[\begin{array}{c} B_x^{\rm T}(q_x,\ \omega) \\ C_x^{\rm T}(q_x,\ \omega) \end{array}\right]_{\rm p}=\frac{\beta_1^{\rm T}(q_x,\ \omega)A_y(q_x,\ \omega)/(\omega\epsilon_0)}{\beta_2^{\rm T}(q_x,\ \omega)+\beta_1^{\rm T}(q_x,\ \omega)\epsilon_2^{\rm T}(q_x,\ \omega)} \times\left[\begin{array}{c} \beta_2^{\rm T}(q_x,\ \omega)-\beta_1^{\rm T}(q_x,\ \omega)\epsilon_2^{\rm T}(q_x,\ \omega) \\ 2\beta_2^{\rm T}(q_x,\ \omega) \end{array}\right], \quad (33)$$

$$\left[\begin{array}{c} B_y^{\rm T}(q_x,\ \omega) \\ C_y^{\rm T}(q_x,\ \omega) \end{array}\right]_{\rm s}=\frac{A_y(q_x,\ \omega)}{\beta_1^{\rm T}(q_x,\ \omega)+\beta_2^{\rm T}(q_x,\ \omega)} \times\left[\begin{array}{c} \beta_1^{\rm T}(q_x,\ \omega)-\beta_2^{\rm T}(q_x,\ \omega) \\ 2\beta_1^{\rm T}(q_x,\ \omega) \end{array}\right], \quad (34)$$

where $\{B_x^{\rm T},\ B_y^{\rm T}\}$ is related to the reflected field, while $\{C_x^{\rm T},\ C_y^{\rm T}\}$ is related to the transmitted field. For the p-polarization, the real part of the pole, *i.e.* $\Re e[\beta_2^{\rm T}(q_x,\ \omega)+\beta_1^{\rm T}(q_x,\ \omega)\epsilon_2^{\rm T}(q_x,\ \omega)]=0$, defines the dispersion relation of the surface-plasmon-polariton (SPP) modes. Assuming a

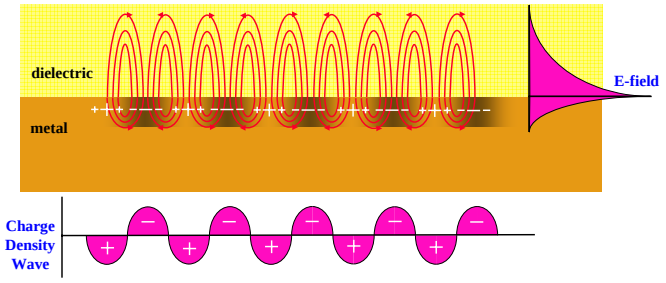

Fig. 12. The upper panel illustrates the electric-field distribution for surface-plasmon-polariton modes, and the lower panel illustrates the charge-density wave for localized surface-plasmon mode.

lossless metal for $\omega \ll \Omega_{3D}^{pl}$, we simply take $\epsilon_2^T(q_x,\ \omega) = 1 - (\Omega_{3D}^{pl}/\omega)^2 < 0$. By using the relations $\beta_1^T(q_x,\ \omega) = \sqrt{(\omega/c)^2 - q_x^2}$ and $\beta_2^T(q_x,\ \omega) = i\sqrt{q_x^2 - (\omega/c)^2\epsilon_2^T(q_x,\ \omega)}$, we get the in-plane wave number of SPP modes [47]

$$k_{spp} = \frac{\omega}{c}\sqrt{\frac{1-(\Omega_{3D}^{pl}/\omega)^2}{2-(\Omega_{3D}^{pl}/\omega)^2}}\ . \tag{35}$$

In the limit of $k_{spp} \to \infty$, we arrive at the localized surface-plasmon (SP) mode [34] with $\Omega_{sp} = \Omega_{3D}^{pl}/\sqrt{2}$. The SP mode is a plasmon excitation that propagates in a charge-density-wave like fashion along the planar interface between a dielectric medium and a metal, whose associated field amplitude decays exponentially with increasing distance into each medium from the interface [47], as shown in Fig. 12. The dipole feature on the interface allows it to couple to the incident radiation field, creating SPP modes. The SPP modes change the incident radiation field into the transmitted near field inside the metal.

In the case of a metal film having two interfaces with air, the previous SP mode is split into one symmetric (+) and one antisymmetric (-) SP modes, given by $\Omega_{sp}^{\pm} = (\Omega_{3D}^{pl}/\sqrt{2})\sqrt{1 \pm \exp(-|q_x|d)}$. Here d is the film thickness.

The excitation of the near field of SPP modes requires a significant momentum k_{spp} along the interface [34]. A simple planar interface cannot satisfy the condition. However, when the interface is either covered with a prism or patterned with a grating [34], the near field of SPP modes can be excited by a normally-incident radiation field on the grating, as shown in Fig. 13.

For the case with the grating, both reflected and transmitted fields possess high-order diffraction modes with a momentum $q_x + n(2\pi/a)$, where $n = 0,\ \pm1,\ \pm2,\ \cdots$ and a is the period of the grating. In addition, the surface grating on top of the interface introduces a standing-wave-like feature in the spatial distribution of the transmitted near field [48], as shown in Fig. 14. For certain frequency ω of the incident light, the transmitted near field will be completely restricted within the gap regions. As a result of the field concentration in the gaps, we expect a very large enhancement of the transmitted field,

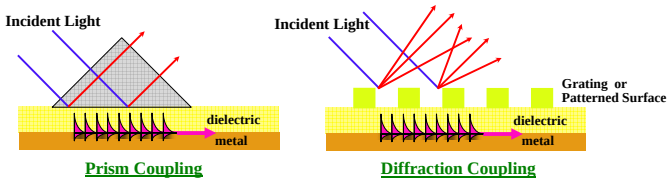

Fig. 13. The left panel illustrates the prism coupling for the excitation of SPP modes, while the right panel illustrates the grating coupling for the excitation of SPP modes.

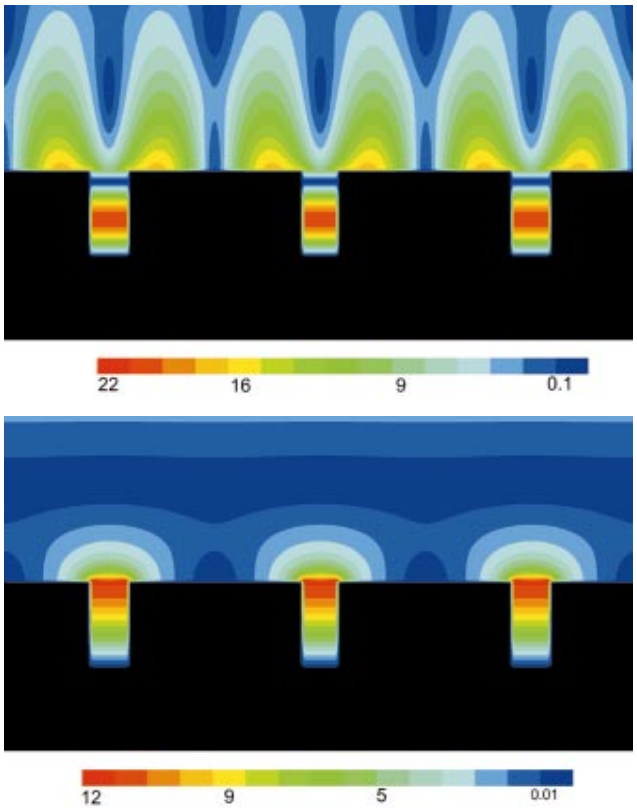

Fig. 14. Plots of the **E** field over three periods of reflection gratings with calculation parameters: $d = 1.75\ \mu m$, $a = 0.3\ \mu m$ and $h = 1.0\ \mu m$. The color scale is the square root of the intensity of the total E field normalized to the incident E field. The two panels correspond to the two resonances with $\lambda_R = 1.8\ \mu m$ for the upper panel and $\lambda_R = 4.6\ \mu m$ for the lower panel. Image used with permission of authors of [48].

which can be used to optically amplify a weakly-incident radiation field.

VI. Conclusion

We have reviewed some possibilities for coherent optical amplification of a normally-incident and weak radiation field using different physical mechanisms, including electronic quantum interference, field enhancement in a photonic crystal and field concentration through surface-plasmon-polariton modes. Some numerical results have been presented for the demonstration of these effects. The important effects due to a longitudinal field associated with the induced three-dimensional plasma wave inside a doped semiconductor are

shown and explained based on a nonlocal and non-adiabatic model.

ACKNOWLEDGMENT

This research was supported by the Air Force Office of Scientific Research (AFOSR).

REFERENCES

[1] P. W. Milonni, "Semiclassical and quantum-electrodynamical approaches in nonrelativistic rediation theory," *Phys. Rep.*, vol. 25, pp. 1-81, 1976.

[2] D. A. Cardimona, M. G. Raymer, and C. R. Stroud Jr., "Steady-state quantum interference in resonance fluorenscence," *J. Phys. B*, vol 15, pp. 55-64, 1982.

[3] A. Imamoğlu and S. E. Harris, "Lasers without inversion: Interference of dressed lifetime-broadened states," *Opt. Lett.* vol. 14, pp. 1344-1346, 1989.

[4] A. Imamoğlu, J. E. Field, and S. E. Harris, "Lasers without inversion: A closed lifetime boradened system," *Phys. Rev. Lett.*, vol. 66, pp. 1154-1156, 1991.

[5] U. Fano, "Effects of configuration interaction on intensities and phase shifts," *Phys. Rev.*, vol. 124, pp. 1866-1878, 1961.

[6] S. E. Harris, "Lasers without inversion: Interference of lifetime-broadened resonances," *Phys. Rev. Lett.*, vol. 62, 1033-1036, 1989.

[7] Y. Zhao, D. H. Huang and C. Wu, "Electric-field induced quantum coherence of the intersubband transition in semiconductor quantum wells," *Opt. Lett.*, vol. 19, pp. 816-818, 1994.

[8] P. Sheng, *Scattering and Localization of Classical Waves in Random Media*, World Scientific, Singapore, 1990.

[9] S. John, "Electromagnetic absorption in a disordered medium near a photon mobility edge," *Phys. Rev. Lett.*, vol. 53, pp. 2169-2172, 1984; "Localization and absorption of waves in a weakly dissipative disordered medium," *Phys. Rev. B*, vol. 31, pp. 304-309, 1985.

[10] P. Sheng and Z. Q. Zhang, "Scalar-wave localization in a two-component composite," *Phys. Rev. Lett.*, vol. 57, pp. 1879-1882, 1986.

[11] K. Ayra, Z. B. Su and J. L. Birman, "Anderson localization of electromagnetic waves in a dielectric medium of randomly distributed metal particles," *Phys. Rev. Lett.*, vol. 57, pp. 2725-2728, 1986.

[12] C. A. Condat and T. R. Kirkpatrick, "Observability of acoustical and optical localization," *Phys. Rev. Lett.*, vol. 58, pp. 226-229, 1987.

[13] C. M. Soukoulis, E. N. Economou, G. S. Grest and M. H. Cohen, "Existence of anderson localization of classical waves in a random two-component medium," *Phys. Rev. Lett.*, vol. 62, pp. 575578, 1989; E. N. Economou and C. M. Soukoulis, "Calculation of optical transport and localization quantities," *Phys. Rev. B*, vol. 40, pp. 7977-7980, 1989.

[14] S. John, "Strong localization of photons in certain disordered dielectric superlattices," *Phys. Rev. Lett.*, vol. 58, pp. 2486-2489, 1987; S. John and R. Rangavajan, "Optimal structures for classical wave localization: an alternative to the ioffe-regel criterion," *Phys. Rev. B*, vol. 38, pp. 10101-10104, 1988.

[15] E. N. Economou and A. Zdetsis, "Classical wave propagation in periodic structures," *Phys. Rev. B*, vol. 40, pp. 1334-1337, 1989.

[16] E. Yablonovitch, "Inhibited spontaneous emission in solid-state physics and electronics," *Phys. Rev. Lett.*, vol. 58, pp. 2059-2062, 1987.

[17] E. Yablonovitch and T. J. Gmitter, "Photonic band structure: The face-centered-cubic case," *Phys. Rev. Lett.*, vol. 63, pp. 1950-1953, 1989; E. Yablonovitch, in *Analogies in Optics and Micro Electronics*, edited by W. van Haeringen and D. Lenstra, Kluwer Academic, The Netherlands, 1990, pp. 117133.

[18] S. Satpathy, Ze Zhang and M. R. Salehpour, "Theory of photon bands in three-dimensional periodic dielectric structures," *Phys. Rev. Lett.*, vol. 64, pp. 1239-1242, 1990; and *Phys. Rev. Lett.*, vol. 65, p. 2478(E), 1990.

[19] K. M. Leung and Y. F. Liu, "Photon band structures: The plane-wave method," *Phys. Rev. B*, vol. 41, pp. 10188-10190, 1990.

[20] K. M. Ho, C. T. Chan and C. M. Soukoulis, "Existence of a photonic gap in periodic dielectric structures," *Phys. Rev. Lett.*, vol. 65, pp. 3152-3155, 1990.

[21] S. Y. Lin, J. G. Fleming and I. El-Kady, "Highly efficient light emission at $\lambda = 1.5$ μm by a three-dimensional tungsten photonic crystal," *Opt. Lett.*, vol. 28, pp. 1683-1685, 2003.

[22] T. W. Ebbesen, H. J. Lezec, H. F. Ghaemi, T. Thio, and P. A. Wolff, "Extrodinary optical transmission through sub-wavelength hole arrays," *Nature*, vol. 391, pp. 667-669, 1998; H. F. Ghaemi, T. Thio, D. E. Grupp, T. W. Ebbesen, and H. J. Lezec, "Surface plasmons enhance optical transmission through subwavelength holes," *Phys. Rev. B*, vol. 58, pp. 6779-6782, 1998.

[23] U. Schröter and D. Heitmann, "Surface-plasmon-enhanced transmission through metallic gratings," *Phys. Rev. B*, vol. 58, pp. 15419-15421, 1998.

[24] R. Dragila, B. Luther-Davies, and S. Vukovic, "High transparency of classically opaque metallic films," *Phys. Rev. Lett.*, vol. 55, pp. 1117-1120, 1985.

[25] A. Barbara, P. Quémerais, E. Bustarret, and T. Lopez-Rios, "Optical transmission through subwavelength metallic gratings," *Phys. Rev. B*, vol. 66, pp. 161403(4), 2002.

[26] P. A. Kossyrev, A. Yin, S. G. Cloutier, D. A. Cardimona, D. H. Huang, P. M. Alsing and J. M. Xu, "Electric field tuning of plasmonic response of nanodot array in liquid crystal matrix," *Nano Lett.*, vol. 5, pp. 1978-1981, 2005.

[27] J. Chandezon, M. T. Dupuis, G. Cornet, and D. Maystre, "Multicoated gratings: a differential formalism applicable in the entire optical region," *J. Opt. Soc. Am.*, vol. 72, pp. 839-846, 1982; W. L. Barnes, T. W. Preist, S. C. Kirtson, and J. R. Sambles, "Physical origin of photonic energy gaps in the propagation of surface plasmons on gratings," *Phys. Rev. B*, vol. 54, pp. 6227-6244, 1996.

[28] S. A. Darmanyan and A. V. Zayats, "Light tunneling via resonant surface plasmon polariton states and the enhanced transmission of periodically nanostructured metal films: An analytical study," *Phys. Rev. B*, vol. 67, pp. 035424(7), 2003; S. A. Darmanyan, M. Nevière, and A. V. Zayats, "Analytical theory of optical transmission through periodically structured metal films via tunnel-coupled surface polariton modes," *Phys. Rev. B*, vol. 70, pp. 075103(9), 2004.

[29] T. Namiki, "3D ADI FDTD method-unconditionally stable time-domain algorithm for solving full vector Maxwell's equations," *IEEE Trans. Microwave Theory Tech.*, vol. 48, pp. 1743-1748, 2000.

[30] S. Das Sarma and J. J. Quinn, "Collective excitations in semiconductor superlattices," *Phys. Rev. B*, vol. 25, pp. 7603-7618, 1982.

[31] D. H. Huang, Y. Zhu, and S. X. Zhou, "Surface plasmons with a gap in a semi-infinite HgTe-CdTe superlattice," *J. Phys.: Condens. Matter*, vol. 1, pp. 7619-7625, 1989.

[32] D. H. Huang, C. Rhodes, P. M. Alsing and D. A. Cardimona, "Effects of longitudinal field on transmitted near field in doped semi-infinite semiconductors with a surface conducting sheet," *J. Appl. Phys.*, vol. 100, 2006.

[33] V. M. Agranovich and D.L. Mills, *Surface Polaritons*, North-Holland, Amsterdam, 1982.

[34] H. Raether, *Surface Plasmons on Smooth and Rough Surfaces and on Gratings*, Springer-Verlag, Berlin, 1988.

[35] A.D. Boardman, *Electromagnetic Surface Modes*, John Wiley & Sons, New York, 1982.

[36] A. V. Zayats and I. I. Smolyaninov, "Near-field photonics: surface plasmon polaritons and localized surface plasmons," *J. Opt. A: Pure Appl. Opt.*, vol. 5, pp. S16-S50, 2003.

[37] G. Boisde and A. Harmer, *Chemical and Biochemical Sensing with Optical Fibers and Waveguides*, Arthech House, Boston, 1996.

[38] H.-E. Ponath and G.I. Stegeman, *Nonlinear Surface Electromagnetic Phenomena*, North-Holland, Amsterdam, 1991.

[39] S. A. Maier, M. L. Brongersma, P. G. Kik, S. Meltzer, A. A. G. Requicha and H. A. Atwater, "Plasmonics - A Route to Nanoscale Optical Devices," *Advanced Materials*, vol. 13, pp. 1501-1505, 2001.

[40] D. A. Cardimona and D. H. Huang, "Connection of off-diagonal radiative-decay coupling to electromagnetically-induced transparency and amplification without inversion in three-level atomic system," *Phys. Rev. A*, vol. 65, pp. 033828(9), 2002.

[41] D. H. Huang and D. A. Cardimona, "Effects of off-diagonal radiative-decay coupling on electron transitions in resonant double quantum wells," *Phys. Rev. A*, vol. 64, pp. 013822(20), 2001.

[42] D. H. Huang and D. A. Cardimona, "Intersubband laser coupled three-level asymmetric quantum wells: New dynamics of quantum interference," *J. Opt. Soc. Am. B*, vol. 15, pp. 1578-1584, 1998.

[43] H. Sami Sözüer and J. W. Haus, "Photonic bands: simple-cubic lattice," *J. Opt. Soc. Am. B*, vol. 10, pp. 296-302, 1993.

[44] K. M. Leung, "Defect modes in photonic band structures: A Green's function approach using vector Wannier functions," *J. Opt. Soc. Am. B*, vol. 10, pp. 303-306, 1993.

[45] F. Forstmann and R. R. Gerhardts, *Metal Optics Near the Plasma Frequency*, Springer-Verlag, Berlin, 1986.

[46] F. Stern, "Polarizability of a Two-Dimensional Electron Gas," *Phys. Rev. Lett.*, vol. 18, pp. 546-548, 1967.

[47] A. V. Zayats, I. I. Smolyaninov and A. A. Maradudin, "Nano-optics of surface plasmon polaritons," *Phys. Rep.*, vol. 408, pp. 131-314, 2005.

[48] F. J. Garcia-Vidal and L. Martin-Moreno, "Transmission and focusing of light in one-dimensional periodically nanostructured metals," *Phys. Rev. B*, vol. 66, pp. 155412(10), 2002.

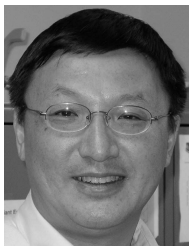

Danhong Huang received the B.S. and M.S. degrees in physics from the Shanghai University of Science and Technology, China in 1984 and 1987, respectively, and the Ph.D. degree in physics from the Fudan University, China in 1990.

Dr. Huang was a Canadian NSERC International Postdoctoral Fellow from 1990-1993 working on many-body effects on quantum transport and optical spectrum, a Research Assistant Professor at the Wayne State University from 1993-1995 working on electronic quantum interference in semiconductor quantum wells, an NRC Research Fellow at the Air Force Research Laboratory from 1995-1997 working on semiconductor IR photodetectors, IPA Research Physicist at the Air Force Research Laboratory from 1997-2001 working on magneto-quantum transport and magneto-optical absorption in low-dimensional semiconductor systems. He has been a research scientist at the US Air Force Research Lab since 2001. His research interests include many-body theory and semiconductor device physics for optics, electronics and optoelectronics.

Dr. Huang is a member of APS and SPIE, has more than 100 publications in referred journals.

D. A. Cardimona received his B.S. in physics and math from Marquette University, Milwaukee, WI in 1976. He earned his Ph.D. in optics from the Institute of Optics at the University of Rochester, Rochester, NY in 1983.

As an undergraduate, he spent a half year at Fermilab helping a team of researchers search for charmed particles. After receiving his advanced degree, he was hired by the Air Force Weapons Laboratory, now the Air Force Research Laboratory, in Albuquerque, NM. As a theoretical Research Physicist, he has over twenty years of experience in quantum and nonlinear optics, with over 50 papers published in refereed journals and four patents. For the past fourteen years, he has performed research in semiconductor heterostructure devices, emphasizing detectors for space applications.

Dr. Cardimona is a member of SPIE. He has received eight Scientific Achievement awards, four Dept. of the Air Force Suggestion awards, the Giller Award for Outstanding Technical Achievement, two Notable Achievement awards, three directorate team awards for Best Paper of the Year, and will be listed in the Marquis' Who's Who in America for 2006.

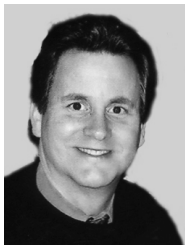

Paul M. Alsing received his B.S. in astrophysics from Michigan State University in 1979, his Masters in physics from the University of New Mexico in 1986, and his Ph.D in quantum optics from University of Arkansas in 1991.

After an NSF postdoctoral fellowship at the University of Canberra, Australia 1991-1992, he was an NRC fellow at the Air Force Research Laboratory from 1992-1995 working on chaotic control and synchronization. From 1995-2005 he was a senior research physicist at the University of New Mexico's High Performance Computing Center, specializing in computational physics on parallel computers. In 2005 he re-joined the Air Force Research Laboratory as a research scientist.

Dr. Alsing's research interests include quantum optics, quantum information and quantum computation, electron-phonon-photon processes in semiconductors, and high performance computational physics. He is a member of the APS and AAPT, has over 60 publications, and has received three directorate team awards for Best Paper for the Year.

DISTRIBUTION LIST

DTIC/OCP
8725 John J. Kingman Rd, Suite 0944
Ft Belvoir, VA 22060-6218 1 cy

AFRL/RVIL
Kirtland AFB, NM 87117-5776 2 cys

Official Record Copy
AFRL/RVSS/D.A. Cardimona 1 cy